Human-Inspired Underactuated Bipedal Robotic Walking with AMBER on Flat-ground, Up-slope and Uneven Terrain

Shishir Nadubettu Yadukumar, Murali Pasupuleti and Aaron D. Ames

***Abstract*— This work presents human-inspired control strategies required for achieving three motion primitives in walking—flat-ground, uneven terrain and up-slope—in an underactuated physical bipedal robot: AMBER. Formal models and controllers which provably guarantee the stability of walking are developed and verified in the simulation. Computationally tractable conditions are given that allow for the experimental implementation of these formal methods through the closed form approximation of constraints that restrict maximum torque, maximum velocity and ensure proper foot clearance. Considering the special property of the motors used in the robot, i.e., low leakage inductance and high angular speed, we approximate the motor model and translate the formal controllers satisfying these constraints into an efficient voltage-based controller that can be directly implemented on AMBER. The end result is robotic walking on AMBER for the three motion primitives that shows good agreement with the formal results from which it was derived.**

I. INTRODUCTION

Humans are exceptional at adapting their walking gait based on the nature of terrain; this enables them to navigate varieties of locations with ease. Hence to achieve bipedal robotic walking which can display various motion primitives, i.e., walking on flat-ground, slopes, stairs and uneven terrain, it is natural to look to human-data for inspiration in the design of formal controllers. In addition, despite the complexity present in the human locomotion system, there is evidence to suggest that humans appear to be controlled (at least in part) by central pattern generators in the spinal cord [8]. This implies that humans may employ potentially characterizable control strategies and the proper representation of human walking can be obtained by studying human walking data.

Motivated by these considerations, recent work by the authors [2], [3], [4] have looked to human walking data to compute outputs that appear to characterize human walking behaviors which can be described by simple functions of time, termed the *canonical walking function*, that gives intuition into these behaviors. Using these constructions, a controller can be implemented that drives the outputs of the robot to the outputs of the human as represented by the canonical walking function. These ideas were formally explored in the case of underactuated bipedal robotic walking, where a *human-inspired* optimization problem was presented (in [3]) that provably resulted in robotic walking on flat ground (in [15]) with the bipedal robot AMBER.

This work is supported by NSF grants CNS-0953823 and CNS-1136104 and NHARP award 00512-0184-2009

S. Nadubettu Yadukumar and M. Pasupuleti are with the Department of Electrical Engineering, Texas A& M University, College Station, TX 77843, USA {muralikris,shishirny}@tamu.edu

A. D. Ames is with the faculty of the Department of Mechanical Engineering and the Department of Electrical Engineering, Texas A & M University, College Station, TX 77843, USA aames@tamu.edu

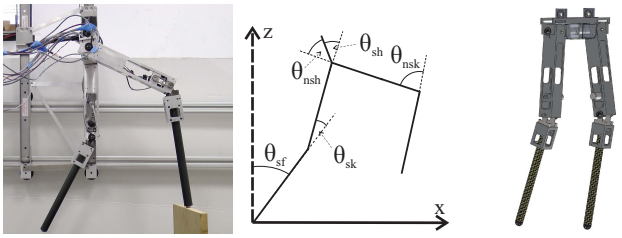

Fig. 1: The biped AMBER (left), the angle conventions (center), and the SolidWorks model of AMBER (right).

The main contribution of this paper is to design experimentally realizable control laws to achieve walking with AMBER (Fig. 1) for three different kinds of motion primitives: flat-ground, rough terrain and up-slope. We begin by introducing a formal model of AMBER, including both its mechanical and electrical components in Sect. II; the fidelity of this model is essential for predicting experimental behavior through simulation. The construction of human-inspired controllers is then presented in Sect. III, along with the human output data that motivated this construction. The main formal result of this paper is presented in Sect. IV: additional constraints to the human-inspired optimization (which are computationally efficient) that will allow the formal results from [3] to be realized experimentally, for different walking behaviors, in a robust fashion. The experimental results are presented in Sect. IV, where we define a voltage-based proportional control law–utilizing only the human outputs and the canonical walking function with parameters obtained from the human-inspired optimization–for which we obtain walking in simulation for all three motion primitives. Good agreement between the simulation and experimentation is seen, indicating that the formal ideas presented can be successfully translated to real-world implementation.

It is important to note that this work has drawn inspiration from work related to: creating low-dimensional representations of human walking through virtual constraints [6], [13]; representations of bipedal robots that attempt to find the underlying simplicity in walking such as single-leg hoppers [12]; the Spring Loaded Inverted Pendulum (SLIP) models [7], [11] for running robots; finally, and most importantly, work that uses virtual constraints and hybrid dynamics to achieve low-dimensional representations of robotic walking [9], [14] that can be realized experimentally [10].

II. BIPEDAL ROBOTIC MODEL

AMBER is a 2D bipedal robot with five links (two calves, two thighs and a torso, see Fig. 2). AMBER is 61 cm tall with a total mass of 3.3 kg (see Fig. 2). While the knees and hips are powered by DC motors, the feet are pointed; and thus are underactuated. AMBER walks in the sagittal plane and its movement in the coronal plane is restricted by the boom (see Fig. 2). In addition, the whole robot ambulates on a treadmill. In this manner, we can also achieve slope walking by just changing the slope (γ) of the treadmill.

Define the configuration space Q with $\theta = (\theta_{sf}.\theta_{sk}, \theta_{sh}, \theta_{nsh}, \theta_{nsk})^T \in Q$ containing the relative angles between links as shown in Fig. 1. When the foot hits the ground, the stance and non-stance legs are swapped. Formally, we represent the robot as a hybrid system (see [2], [3] for details) indexed by ground slope γ:

$$\mathscr{HC}_\gamma = (X_\gamma, U, S_\gamma, \Delta, f, g), \tag{1}$$

where $X_\gamma \subset TQ$ is the domain, $U \subset \mathbb{R}^4$ is the set of admissible controls, $S_\gamma \subset X_\gamma$ is the guard, and Δ is the reset map. $(f(x), g(x))$ forms a control system, i.e., $\dot{x} = f(x) + g(x)u$.

Continuous Dynamics. Calculating the inertial properties of each link of the robot (Fig. 1) yields the Lagrangian, $L(\theta, \dot{\theta}) = \frac{1}{2}\dot{\theta}^T D(\theta)\dot{\theta} - V(\theta)$. The inertias of the motors and boom are also included. Let I_r, I_g, I_m be the rotational inertias of the rotor, gearbox, and motor, respectively. Then, $I_m = I_r r^2 + I_g$, where $r = 157$ is the gear ratio. Because r is large, I_g can be ignored. Each joint is connected to a motor through a metal chain. Therefore, the axis of rotation of the rotor has an offset w.r.t. that of the link. Using the parallel axis theorem: $I_p = I_m + m_m d_m^2$, where I_p is the motor inertia shifted to the joint axis, m_m is the mass of the rotating motor parts, and d_m is the distance between axes. Again, since $m_m = 0.011$ kg, $I_p \approx I_m$.

The boom is rigidly bolted to the sliders and thus does not rotate w.r.t. the world frame. Therefore, only the translational inertia of the boom is considered. Let m_x (resp. m_z) denote the mass of the parts in the boom-slider moving forward and backward (resp. upward and downward). Then, the resulting mass matrix is $M_{boom} \in \mathbb{R}^{6\times 6}$ where $(M_{boom})_{1,1} = m_x$ and $(M_{boom})_{3,3} = m_z$ with all other entries equal to zero. The combined inertia matrix, D_{com}, used in the Lagrangian is

$$D_{com}(\theta) = D(\theta) + \text{diag}(0, I_{m,sk}, I_{m,sh}, I_{m,nsh}, I_{m,nsk}) + J(\theta)^T M_{boom} J(\theta), \tag{2}$$

where $I_{m,sk}$, $I_{m,sh}$, $I_{m,nsh}$, $I_{m,nsk}$ represent the motor inertias of the links and $J(\theta)$ is the body Jacobian of the torso center of mass. The Euler-Lagrange equation yields a dynamic model:

$$D_{com}(\theta)\ddot{\theta} + H(\theta, \dot{\theta}) = B(\theta)u, \tag{3}$$

where the control, u, is a vector of torque inputs. Since AMBER has DC motors, we need to derive equations with voltage inputs. Since the motor inductances are small, we can realize the electromechanical system:

$$V_{in} = R_a i_a + K_\omega \omega, \tag{4}$$

where V_{in} is the vector of voltage inputs to the motors, i_a is the vector of currents through the motors, and R_a is the resistance matrix. Since the motors are individually controlled, R_a is a diagonal matrix. K_ω is the motor constant matrix and ω is a vector of angular velocities of the motors. Representing (4) in terms of currents, the applied torque is $u = K_\varphi R_a^{-1}(V_{in} - K_\omega \omega)$, with K_φ the torque constant matrix. Thus, the Euler-Lagrange equation takes the form $D_{com}(\theta)\ddot{\theta} + H(\theta, \dot{\theta}) = B(\theta)K_\varphi R_a^{-1}(V_{in} - K_\omega \omega)$.

Converting this model to first order ODEs yields the affine control system (f_v, g_v) with inputs V_{in}:

$$f_v(\theta, \dot{\theta}) = \begin{bmatrix} \dot{\theta} \\ -D_{com}^{-1}(\theta)(H(\theta, \dot{\theta}) + B(\theta)K_\varphi R_a^{-1} K_\omega \omega) \end{bmatrix},$$
$$g_v(\theta) = \begin{bmatrix} \mathbf{0} \\ D_{com}^{-1}(\theta)B(\theta)K_\varphi R_a^{-1} \end{bmatrix}. \tag{5}$$

Discrete Dynamics. The domain, X_γ, describes the allowable state space restricted by the guard, h_γ. For AMBER, the non-stance foot must be above a slope of γ, i.e., $h_\gamma \geq 0$:

$$X_\gamma = \left\{(\theta, \dot{\theta}) \in TQ : h_\gamma(\theta) \geq 0\right\},$$

The guard is just the boundary of the domain with the additional assumption that h_γ is decreasing:

$$S_\gamma = \left\{(\theta, \dot{\theta}) \in TQ : h_\gamma(\theta) = 0 \text{ and } dh_\gamma(\theta)\dot{\theta} < 0\right\},$$

with $dh_\gamma(\theta)$ the Jacobian of h_γ at θ. When the non-stance foot impacts the ground, the angular velocities change. Hence we define a reset map, $\Delta : S_\gamma \to X_\gamma$ which maps the pre-impact state to the post-impact state; see [2] for details.

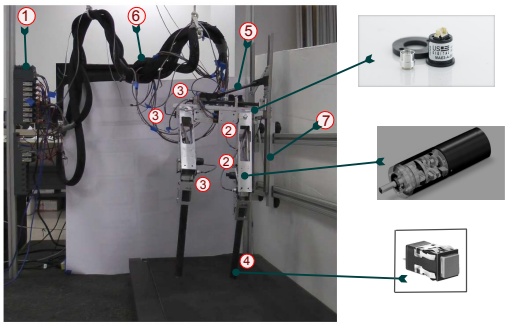

Model Parameters				
Parameter	Mass g	Length mm	Inertia x-axis $\times 10^3$ $g\,mm^2$	Inertia z-axis $\times 10^3$ $g\,mm^2$
Stance calf	213.79	312.27	1967.37	119.69
Stance knee	606.15	282.37	6494.94	418.37
Torso	804.83	9.97	3730.23	3577.19
Non-stance knee	606.15	282.37	6494.94	418.37
Non-stance calf	213.79	312.37	1967.37	119.69

Fig. 2: Amber Experimental Setup. Parts marked are (**1**): NI cRIO, (**2**): Maxon DC Motors located in the calf and the torso, (**3**): Encoders on boom and the joints, (**4**): Contact switch at the end of the foot, (**5**): Boom, (**6**): Wiring with sheath protection, (**7**): Slider for restricting the motion to the sagittal plane. The table contains the properties of each link.

III. HUMAN-INSPIRED CONTROL

This section reviews *human-inspired control* so as to properly frame the formal results that are utilized to experimentally achieve robotic walking. Specifically, we review the formal results from [3] (also see [2], [4] for related results in the case of full actuation), that will be coupled with a novel method to ensure the practical realizability of these results.

Human Outputs and Walking Functions. Since our approach toward achieving walking is inspired by the way humans walk, we begin by considering data from human walking experiments (see [2], [4] for details). Rather than looking to the joint angles of the humans over time as is traditionally done [13], we seek "outputs" of the human that provide a "low-dimensional" representation of human walking. Five outputs are used in this paper: $\delta p_{\text{hip}}(\theta)$, the linearized position of the hip, m_{nsl}, the linearized slope of the non-stance leg, θ_{sk}, the stance knee angle, θ_{nsk}, the non-stance knee angle, and $\theta_{tor}(\theta)$, the torso angle from vertical. These outputs are shown in Fig. 3. See [4] for more details.

We make the following observations from the human data: The linearized position of the hip is a linear function of time.

$$\delta p^d_{\text{hip}}(t,v) = v_{hip} t, \tag{6}$$

The other outputs appear to act like the time solution to linear mass-spring-damper systems which motivates the introduction of the *canonical walking function (CWF)*:

$$y_H(t,\alpha) = e^{-\alpha_1 t}(\alpha_2 \cos(\alpha_3 t) + \alpha_4 \sin(\alpha_3 t)) + \alpha_5, \tag{7}$$

with $\alpha_1 = c_0$, $\alpha_2 = \omega_d$, $\alpha_3 = c_1$, $\alpha_4 = \zeta\omega_n$ and $\alpha_5 = g$, with damping ratio ζ, natural frequency ω_n, and damped natural frequency $\omega_d = \omega_n\sqrt{1-\zeta^2}$, and c_0 and c_1 found from initial conditions, and g a gravity-related constant. This function

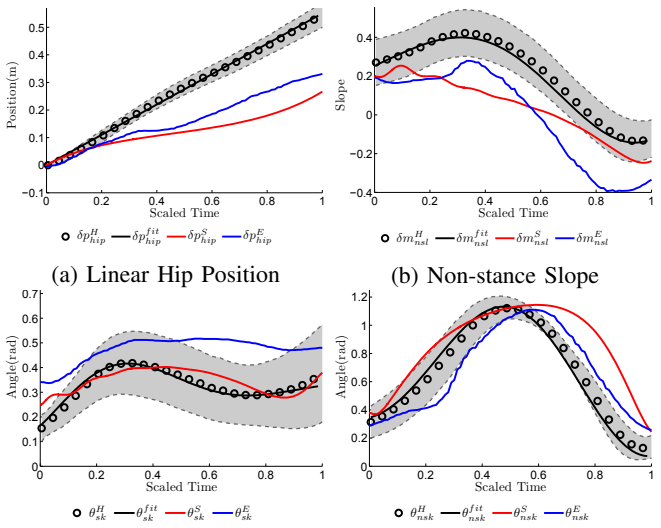

(a) Linear Hip Position (b) Non-stance Slope

(c) Stance Knee (d) Non-stance Knee

Fig. 3: Human output data and the corresponding canonical walking function fits (black) compared against the simulated (red) and experimental (blue) robotic walking.

has the capacity to represent humanlike walking. This is the essence of Human-Inspired Control.

Human-Inspired Outputs. Having defined the outputs, the goal will be to construct a controller that drives the outputs of the robot to the outputs of the human, as represented by the *CWF*: $y_a(\theta(t)) \to y_d(t,\alpha)$, with:

$$\begin{aligned} y_d(t,\alpha) &= [y_H(t,\alpha_{nsl}), y_H(t,\alpha_{sk}), y_H(t,\alpha_{nsk}), y_H(t,\alpha_{tor})]^T, \\ y_a(\theta) &= [\delta m_{nsl}(\theta), \theta_{sk}, \theta_{nsk}, \theta_{tor}(\theta)]^T, \end{aligned}$$

where $y_H(t,\alpha_i)$, $i \in \{nsl, sk, nsk, tor\}$ is the *CWF* (7) but with parameters α_i specific to the output being considered. Grouping these parameters with the velocity of the hip, v_{hip}, that appears in (6), results in the vector of parameters $\alpha = (v_{hip}, \alpha_{nsl}, \alpha_{sk}, \alpha_{nsk}, \alpha_{tor}) \in \mathbb{R}^{21}$.

In order to remove the dependence of time in $y_d(t,\alpha)$ we introduce a parameterization based upon the fact that the (linearized) position of the hip is accurately described by a linear function of time:

$$\tau(\theta) = (\delta p^R_{\text{hip}}(\theta) - \delta p^R_{\text{hip}}(\theta^+))/v_{\text{hip}}, \tag{8}$$

where $\delta p^R_{\text{hip}}(\theta^+)$ is the linearized position of the hip at the beginning of a step. θ^+ is the configuration where the height of the non-stance foot is zero, i.e., $h_\gamma(\theta^+) = 0$. Using (8), we define the following *human-inspired* output:

$$y_\alpha(\theta) = y_a(\theta) - y_d(\tau(\theta), \alpha). \tag{9}$$

Control Law Construction. Consider again the affine control system (f,g) associated with (1). The outputs were chosen so that the decoupling matrix, $A(\theta,\dot\theta) = L_g L_f y_\alpha(\theta,\dot\theta)$ with L the Lie derivative, is nonsingular. Therefore, the outputs have (vector) relative degree 2 and we can define the following torque controller:

$$\begin{aligned} &u_{(\alpha,\varepsilon)}(\theta,\dot\theta) = \\ &-A^{-1}(\theta,\dot\theta)\left(L_f^2 y_\alpha(\theta,\dot\theta) + 2\varepsilon L_f y_\alpha(\theta,\dot\theta) + \varepsilon^2 y_\alpha(\theta)\right). \end{aligned} \tag{10}$$

In other words, we can apply feedback linearization to obtain the linear system on the human-inspired output: $\ddot y_\alpha = -2\varepsilon\dot y_\alpha - \varepsilon^2 y_\alpha$. This system is exponentially stable, implying that for $\varepsilon > 0$ the control law $u_{(\alpha,\varepsilon)}$ drives $y_\alpha \to 0$ as $t \to \infty$. Applying the feedback control law in (10) to the hybrid control system, $\mathscr{HC}$ as given in (1), yields a hybrid system:

$$\mathscr{H}_\gamma^{(\alpha,\varepsilon)} = (X_\gamma, S_\gamma, \Delta, f^{(\alpha,\varepsilon)}), \tag{11}$$

where, X_γ, S_γ, and Δ are defined as for $\mathscr{HC}_\gamma$, and

$$f^{(\alpha,\varepsilon)}(\theta,\dot\theta) = f(\theta,\dot\theta) + g(\theta,\dot\theta)u_{(\alpha,\varepsilon)}(\theta,\dot\theta).$$

Human-Inspired Hybrid Zero Dynamics The controller (10) drives $y_a \to y_d$, or it renders the *zero dynamics surface*:

$$\mathbf{Z}_\alpha = \{(\theta,\dot\theta) \in TQ : y_\alpha(\theta) = \mathbf{0},\ L_f y_\alpha(\theta,\dot\theta) = \mathbf{0}\} \tag{12}$$

invariant for the continuous dynamics. But, the discrete impacts in the system cause the state to be "thrown off" of the zero dynamics surface. Therefore, a hybrid system has *hybrid zero dynamics* if the zero dynamics is invariant through impact: $\Delta(S_\gamma \cap \mathbf{Z}_\alpha) \subset \mathbf{Z}_\alpha$. With the goal of restating

this in a way that is independent of state variables (position and velocity), we can use the outputs and guard to explicitly solve for the configuration of the system $\vartheta(\alpha) \in Q$ on the guard in terms of the parameters, α. In particular, let

$$\begin{aligned} \vartheta(\alpha) = \theta \qquad \text{s.t} \qquad & \begin{bmatrix} y_\alpha(\Delta_\theta \theta) \\ h_\gamma(\theta) \end{bmatrix} = \begin{bmatrix} \mathbf{0} \\ 0 \end{bmatrix}, \qquad (13) \\ \dot{\vartheta}(\alpha) \qquad = \qquad & \begin{bmatrix} d\delta p^R_{\text{hip}}(\vartheta(\alpha)) \\ dy_\alpha(\vartheta(\alpha)) \end{bmatrix}^{-1} \begin{bmatrix} v_{\text{hip}} \\ \mathbf{0} \end{bmatrix}, \end{aligned}$$

where Δ_θ is the relabeling matrix and $d\delta p^R_{\text{hip}}(\theta)$ and $dy_\alpha(\theta)$ the Jacobian of δp_{hip} and y_α, respectively. It follows that $(\vartheta(\alpha), \dot{\vartheta}(\alpha)) \in \mathbf{Z}_\alpha \cap S$ and $\delta \dot{p}^R_{\text{hip}}(\vartheta(\alpha), \dot{\vartheta}(\alpha)) = v_{\text{hip}}$.

IV. HUMAN-INSPIRED OPTIMIZATION

We now present the main formal result (originally introduced in [3], [2], [4]) that will be used to generate the control parameters that will be experimentally implemented on AMBER to obtain robotic walking.

Optimization Theorem. We need to determine the parameters α^* for the *CWF* $y_H(t, \alpha_i)$, $i \in \{nsl, sk, nsk, tor\}$, which give the best fit to the human mean walking data. This calls for defining a cost function, $\text{Cost}_{\text{HD}}(\alpha)$, which is the sum of squared errors between the human data and the *CWF* picked over a set of discrete times (see [2]). Accordingly, we can compute the least squares fit of the mean human output data with the *CWF*:

$$\alpha^* = \underset{\alpha \in \mathbb{R}^{21}}{\text{argmin}} \ \text{Cost}_{\text{HD}}(\alpha) \qquad (14)$$

While this provides an α^* that yields a good fit of the human data (see Fig. 3), these parameters will not result in robotic walking due to the differences between AMBER and humans. Therefore, the goal is to determine these parameters which provide the best fit of the human data while simultaneously guaranteeing stable walking in the robot. This motivates the following theorem (which first appeared in [3]):

Theorem 1: *The parameters α^* solving the constrained optimization problem:*

$$\begin{aligned} \alpha^* = \underset{\alpha \in \mathbb{R}^{21}}{\text{argmin}} \ & \text{Cost}_{\text{HD}}(\alpha) && (15) \\ \text{s.t} \quad & y_\alpha(\vartheta(\alpha)) = \mathbf{0} && \text{(C1)} \\ & dy_\alpha(\Delta_\theta \vartheta(\alpha)) \Delta_{\dot{\theta}}(\vartheta(\alpha)) \dot{\vartheta}(\alpha) = \mathbf{0} && \text{(C2)} \\ & dh(\vartheta(\alpha)) \dot{\vartheta}(\alpha) < 0 && \text{(C3)} \\ & \mathscr{D}_{\mathbf{Z}}(\vartheta(\alpha)) < 0 && \text{(C4)} \\ & 0 < \Delta_{\mathbf{Z}}(\vartheta(\alpha)) < 1 && \text{(C5)} \end{aligned}$$

yield hybrid zero dynamics: $\Delta(S_\gamma \cap \mathbf{Z}_{\alpha^*}) \subset \mathbf{Z}_{\alpha^*}$. Moreover, there exists an $\hat{\varepsilon} > 0$ such that for all $\varepsilon > \hat{\varepsilon}$ the hybrid system $\mathscr{H}_\gamma^{(\alpha^*, \varepsilon)}$ has a stable periodic orbit with fixed point $(\theta^*, \dot{\theta}^*) \in S \cap \mathbf{Z}_{\alpha^*}$ that can be explicitly computed.

It is not possible to explain this theorem in detail, but one can be found in [3], [15]. Of particular importance is the point $(\vartheta(\alpha), \dot{\vartheta}(\alpha)) \in S \cap \mathbf{Z}_\alpha$ which is used to ensure hybrid zero dynamics through (C1)-(C3), and guarantees the existence of a stable periodic orbit in the zero dynamics surface through (C4) and (C5) which implies the existence of a stable walking gait for sufficiently large ε.

Constraints for Experimental Realizability. The walking that we achieve using Theorem 1 should be physically realizable, which necessitates the additional constraints that ensure that the resulting control parameters will experimentally result in walking with AMBER such as foot height, maximum velocity and peak torque constraints. One could directly introduce these constraints, but computing them would then require directly integrating the systems dynamics. This is prohibitive, since when designing walking gaits for the robot the optimization cannot be run just once, but rather must be run thousands of times to find the best, most physically realizable, walking gaits. Therefore, a way of approximately enforcing physical realizability constraints, in closed form, is highly desirable.

The method we utilize is based upon the fact that the conditions in Theorem 1 also imply the existence of a stable walking for fully actuated walking for which $(\vartheta(\alpha), \dot{\vartheta}(\alpha))$ converges to the fixed point of the associated exponentially stable periodic orbit as $\varepsilon \to \infty$ [4]. In addition, since fully actuated walking directly controls the velocity of the hip, $\tau(\theta) \to t$ as $\varepsilon \to \infty$ which implies that $\tau(\vartheta(\alpha)) \to T$ with T the period of a step.

Define $\xi_1 = \delta p^R_{\text{hip}}(\theta)$ and $\xi_2 = \delta \dot{p}^R_{\text{hip}}(\theta, \dot{\theta})$. Note that we can write $\xi_1 = c\theta$ and $y_a(\theta) = H\theta$. In addition, due to the form of $\tau(\theta)$, we can write $y_d(\tau(\theta), \alpha) = y_d(\xi_1, \alpha)$. This allows us to define:

$$\Phi(\xi_1, \alpha) := \begin{bmatrix} c \\ H \end{bmatrix}^{-1} \begin{bmatrix} \xi_1 \\ y_d(\xi_1, \alpha) \end{bmatrix} \qquad (16)$$

$$\Psi(\xi_1, \alpha) := \begin{bmatrix} c \\ H \end{bmatrix}^{-1} \begin{bmatrix} 1 \\ \frac{\partial y_d(\xi_1, \alpha)}{\partial \xi_1} \end{bmatrix} \qquad (17)$$

With the assumption that $\tau(\theta) = t$, it follows that:

$$\xi_1^e(t) := v_{\text{hip}} t + \delta p^R_{\text{hip}}(\Delta_\theta \vartheta(\alpha)), \quad \xi_2^e(t) := v_{\text{hip}} \qquad (18)$$

From which we define our approximate solutions:

$$\theta^e(t, \alpha) = \Phi(\xi_1^e(t), \alpha), \quad \dot{\theta}^e(t, \alpha) = \Psi(\xi_1^e(t), \alpha) \xi_2^e(t). \quad (19)$$

Note that in the case of full actuation, it is fairly easy to prove that this solution converges to the actual solution of the system. Therefore, viewing the fully actuated walking that is implied by Theorem 1 as an "approximation" of the underactuated walking (which is actually a good approximation since there they will have the same configuration at foot strike) we define the following "practical" and easily computable constraints:

(C6): *Foot scuffing prevention*: The height of the non-stance foot at any point of time, must be such that it is greater than a quadratic polynomial, $P(\theta)$:

$$\max_{0 \le t \le \tau(\vartheta(\alpha))} (h_R(\theta^e(t, \alpha)) - P(\theta^e(t, \alpha))) > 0$$

where $P(\theta) = a x_f(\theta)^2 + b x_f(\theta) + c$ with $x_f(\theta)$ is the horizontal position of the swing foot w.r.t the stance foot and $a = -\frac{4h_{max}}{\text{SL}(\alpha)^2}, b = \frac{4h_{max}\text{SL}(\alpha)}{\text{SL}(\alpha)^2}, c = -\frac{4h_{max} x_f(\vartheta(\alpha)) x_f(\Delta(\vartheta(\alpha)))}{\text{SL}(\alpha)^2}$, where

$\mathrm{SL}(\alpha) = x_f(\vartheta(\alpha)) - x_f(\Delta(\vartheta(\alpha)))$ is the step length of the robot, computed from α through $\vartheta(\alpha)$. These constants, therefore, can be adjusted based on the required maximum stance foot height, h_{max}, and step length, $\mathrm{SL}(\alpha)$.

(C7): *Peak torque*: The maximum torque delivered by the motors is limited ($2Nm$ for AMBER). Therefore, the peak torque required during a walking gait must be:

$$\max_{0\le t\le\tau(\vartheta(\alpha))} \|u_{(\alpha,\varepsilon)}(\theta^e(t,\alpha),\dot{\theta}^e(t,\alpha)))\|_\infty < u_{max}$$

with $u_{(\alpha,\varepsilon)}$, dependent on the parameters α and ε, given in (10) and u_{max} the maximum torque of the motors.

(C8): *Hip-Velocity*: The desired hip velocity of the biped is constrained within the limits: $v_{min} < v_{hip} < v_{max}$. For AMBER, $v_{min} = 0.1\mathrm{m/s}$ and $v_{max} = 0.6\mathrm{m/s}$.

(C9): *Angular velocities of joints*: The maximum angular velocities are limited by the motors ($6.5rad/s$):

$$\max_{0\le t\le\tau(\vartheta(\alpha))} \|\dot{\theta}^e(t,\alpha)\|_\infty < \dot{\theta}_{max}$$

V. IMPLEMENTATION AND EXPERIMENT

The human-inspired torque control proposed in the previous section requires us to linearize the dynamics of AMBER through model inversion. This is not only memory intensive, but also computationally demanding. Therefore, we decided to adopt a simple proportional control law (a similar idea was used in [5]) on the outputs and provide the control input in the form of voltage, since the actuators are electric motors. This also becomes very convenient considering the fact that a DC motor "almost" behaves like a linear system; and the inertia of the motor is large when compared to that of its corresponding link (approximately 10 times).

Human-Inspired Voltage Control. Let V_{in} be the vector of voltage inputs to the motors. Define the following human-inspired proportional (P) voltage control law:

$$V_{in} \quad = \quad -K_p y_\alpha(\theta), \tag{20}$$

where K_p is the constant matrix with its diagonal entries being the proportional gains for each of the motors and its non-diagonal entries are zero since the motors are controlled independently. This control law can be applied to the control system defined by (5) modeling the bipedal robot in conjunction with the motors. It is important to note that the order of the voltage inputs in (20) is considered in such a way that each motor directly represents the output it is "intuitively" driving. For example, it is evident that stance-knee voltage, V_{sk}, has direct control over the stance-knee angle and no direct control over the non-stance knee angle. Thus, the order was chosen in such a way that each output was controllable by its corresponding assigned voltage.

Since *flat-ground walking* can be directly translated to walking obtained in [15] by just substituting $\gamma = 0$, we are going to omit it and progress to the other two motion-primitives. Nevertheless, tiles and figures of walking on flat ground (Fig. 6a and Fig. 5) are shown for comparison.

Rough terrain walking: In order to verify the robustness of the walking obtained from the flat-ground optimization

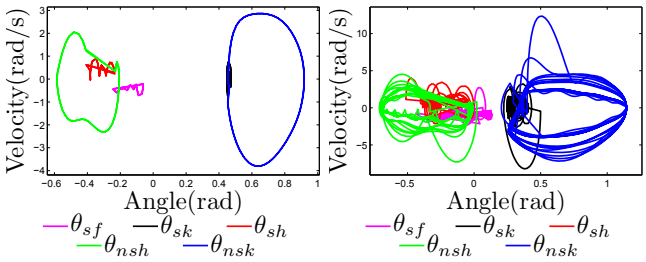

Fig. 4: Phase portraits for the walking gaits found in simulation for up-slope walking with voltage control (left) and flat-ground walking on uneven terrain (right).

i.e., by implementing P-control using α^*, we make the biped walk on rough terrain with a change of 1.94 cm in terrain height. To determine *a priori* the response of the robot to such disturbances, we simulated walking with a 1.94 cm obstacle in the middle of flat terrain by varying the unilateral constraint $h_\gamma(q)$ to get the desired height over the course of the terrain. The resulting phase portrait is shown in Fig. 4 and joint angles are shown in Fig. 5. The biped converges back to stable walking mode after the disturbance, showing the robustness in walking on uneven terrain. Due to space limitations, results of other disturbances conducted on AMBER are omitted (see [1] for the video).

Walking up an incline: Walking on a slope is obtained by solving the optimization problem for a non-zero value of γ. We considered $\gamma = 2^0$, which is reasonable for a robot of the size and power capabilities of AMBER. Again, we get α^*_γ, the solution to the optimization problem in Theorem 1 and apply the voltage control law resulting in stable up-slope walking. The periodic orbit for the walking obtained is shown in Fig. 4, behavior of angles over 10 steps is shown in Fig. 5 and the comparison of slope walking tiles between simulation and experiment can be seen in Fig. 6c. The mismatch is pronounced in stance knee because the motors are capable of only delivering torque of 2Nm. In spite of this limitation, due to inherent robustness of human-inspired control, AMBER could achieve walking on an up-slope.

CONCLUSIONS

This paper achieved walking on three motion primitives by using human-inspired control. From walking tiles and joint angle tracking behavior considered, it can be stated that the physically realizable walking obtained from the simulation is mirrored in the walking obtained in physical world. This speaks to the strength of the formal theory in obtaining experimentally realizable walking. The simplicity of the control law resulted in low computation overhead for the controller implementation thereby enabling us to use a time step of 5ms for each calculation. We can conclude, by observing Fig. 3, that the obtained robotic walking is "human-like", as the experimental outputs match the human output data well. In addition, the walking is also robust to changes in terrain (up to 6cm), change of treadmill speeds (12.5%) and even force disturbances on all of the links.

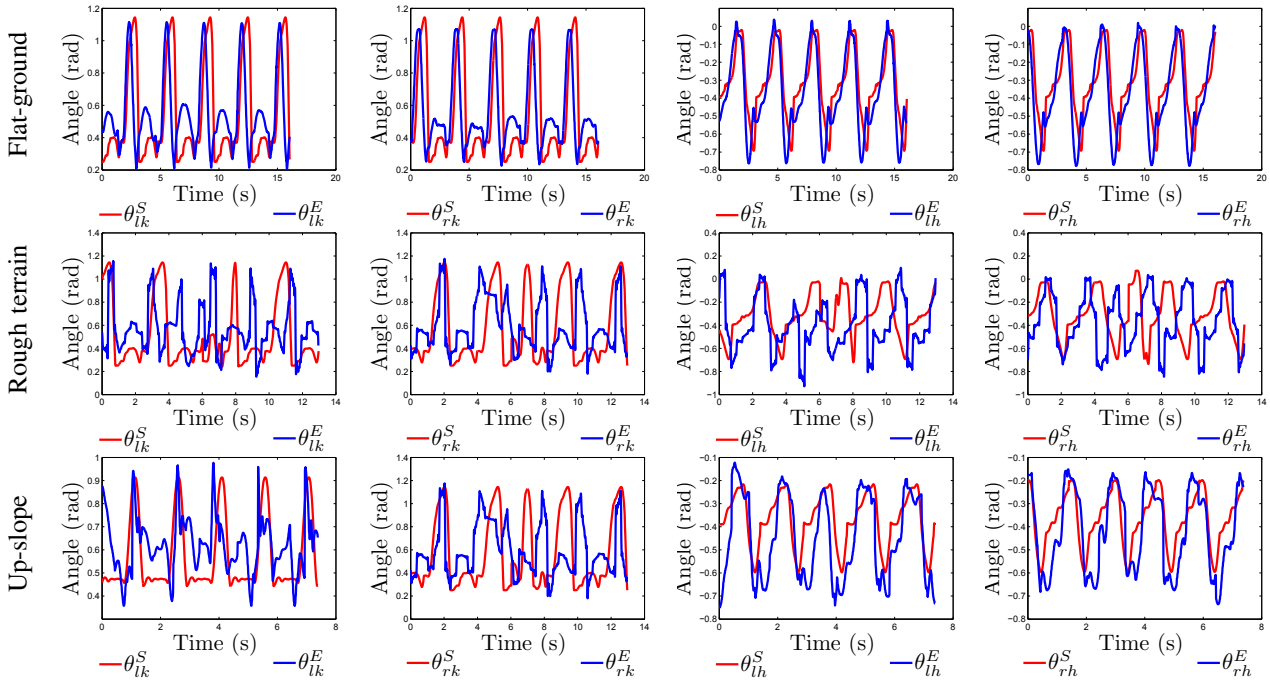

Fig. 5: Experimental (blue) vs. simulated (red) angles over 10 steps for flat-ground, uneven terrain and up-slope walking.

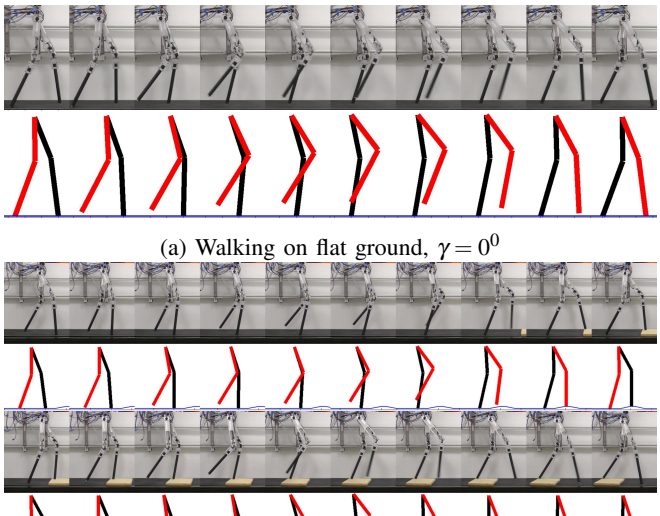

(a) Walking on flat ground, $\gamma = 0^0$

(b) Walking on rough terrain with a disturbance of 1.94 cm

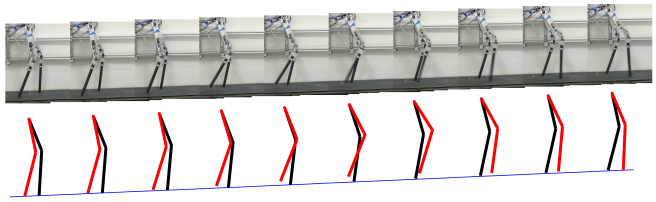

(c) Walking up a slope, $\gamma = 2^0$

Fig. 6: Simulation (bottom) vs Experiment (top) for: (a) flat-ground walking, (b) uneven terrain, (c) up-slope walking.

REFERENCES

[1] AMBER robustness tests. `http://youtu.be/RgQ8atV1NW0`.

[2] A. D. Ames. First steps toward automatically generating bipedal robotic walking from human data. In *Robotic Motion and Control 2011*, volume 422 of *LNICS*, pages 89–116. Springer, 2012.

[3] A. D. Ames. First steps toward underactuated human-inspired bipedal robotic walking. In *2012 IEEE Conference on Robotics and Automation*, St. Paul, Minnesota, 2012.

[4] A. D. Ames, E. A. Cousineau, and M. J. Powell. Dynamically stable robotic walking with NAO via human-inspired hybrid zero dynamics. In *Hybrid Systems: Computation and Control, 2012*, Beijing, China, 2012.

[5] T. Burg, D. Dawson, J. Hu, and M. de Queiroz. An adaptive partial state-feedback controller for RLED robot manipulators. *Automatic Control, IEEE Transactions on*, 41(7):1024 –1030, 1996.

[6] H. Geyer and H. Herr. A muscle-reflex model that encodes principles of legged mechanics produces human walking dynamics and muscle activities. *Neural Systems and Rehabilitation Engineering, IEEE Transactions on*, 18(3):263 –273, 2010.

[7] P. Holmes, R. J. Full, D. Koditschek, and J. Guckenheimer. The dynamics of legged locomotion: Models, analyses, and challenges. *SIAM Rev.*, 48:207–304, 2006.

[8] A. J. Ijspeert. Central pattern generators for locomotion control in animals and robots: a review. *Neural Networks*, 21(4):642–653, 2008.

[9] I. R. Manchester, U. Mettin, F. Iida, and R. Tedrake. Stable dynamic walking over uneven terrain. *The International Journal of Robotics Research*, 30(3):265–279, 2011.

[10] H. Park, K. Sreenath, J. Hurst, and J. W. Grizzle. Identification of a bipedal robot with a compliant drivetrain: Parameter estimation for control design. *IEEE Control Systems Magazine*, 31(2):63–88, 2011.

[11] I. Poulakakis and J. W. Grizzle. The Spring Loaded Inverted Pendulum as the Hybrid Zero Dynamics of an Asymmetric Hopper. *Transaction on Automatic Control*, 54(8):1779–1793, 2009.

[12] M. H. Raibert. Legged robots. *Communications of the ACM*, 29(6):499–514, 1986.

[13] S. Srinivasan, I. A. Raptis, and E. R. Westervelt. Low-dimensional sagittal plane model of normal human walking. *ASME J. of Biomechanical Eng.*, 130(5), 2008.

[14] E. R. Westervelt, J. W. Grizzle, C. Chevallereau, J. H. Choi, and B. Morris. *Feedback Control of Dynamic Bipedal Robot Locomotion*. CRC Press, Boca Raton, 2007.

[15] S. Nadubettu Yadukumar, M. Pasupuleti, and A. D. Ames. From formal methods to algorithmic implementation of human inspired control on bipedal robots. In *Tenth International Workshop on the Algorithmic Foundations of Robotics (WAFR)*, Cambridge, MA, 2012.